Correspondence and
requests for materials
should be addressed to
I.W. (wainer@usp.br)

# Reconstruction of the South Atlantic Subtropical Dipole index for the past 12,000 years from surface temperature proxy

Ilana Wainer[1], Luciana Figueiredo Prado[1], Myriam Khodri[2] & Bette Otto-Bliesner[3]

[1]Instituto Oceanográfico da Universidade de São Paulo, São Paulo, 05508-120, Brazil, [2]Sorbonne Universités (UPMC, Univ Paris 06)-CNRS-IRD-MNHN, LOCEAN Laboratory, 4 place Jussieu, F-75005 Paris, France, [3]Climate and Global Dynamics Division, National Center for Atmospheric Research, Boulder, Colorado 80307, USA.

Climate indices based on sea surface temperature (SST) can synthesize information related to physical processes that describe change and variability in continental precipitation from floods to droughts. The South Atlantic Subtropical Dipole index (SASD) is based on the distribution of SST in the South Atlantic and fits these criteria. It represents the dominant mode of variability of SST in the South Atlantic, which is modulated by changes in the position and intensity of the South Atlantic Subtropical High. Here we reconstructed an index of the South Atlantic Ocean SST (SASD-like) for the past twelve thousand years (the Holocene period) based on proxy-data. This has great scientific implications and important socio-economic ramifications because of its ability to infer variability of precipitation and moisture over South America where past climate data is limited. For the first time a reconstructed index based on proxy data on opposite sides of the SASD-like mode is able to capture, in the South Atlantic, the significant cold events in the Northern Hemisphere at 12.9−11.6 kyr BP and 8.6−8.0 ky BP. These events are related, using a transient model simulation, to precipitation changes over South America.

P recipitation in South America associated with the South American Monsoon system (SAMS) has been the subject of extensive investigation since the 1980s, having become a major field of climate-related research[1]. Many processes are responsible for its variability from time-scales ranging from diurnal to decadal including intensity, timing of onset/demise and spatial extent[2]. One of the forcings that has been recognized as an important player in understanding the variability of the SAMS at seasonal, interannual-to-decadal time scales has been the pattern of sea surface temperature (SST) anomalies of the South Atlantic Ocean[3]. The extent of their influence is still under debate considering that at the same time, SAMS has also been strongly linked to El Niño Southern Oscillation-related (ENSO) SST variability[4]. Nonetheless, it is possible to remove the ENSO signal from the SAMS and the remaining South Atlantic Subtropical Dipole (SASD) SST mode can still explain ca. 20% of its variance[5].

The SASD has a dipole structure oriented in the northeast-southwest direction linked to changes in winds and sea level pressure (SLP)[6–8]. The Northeastern Pole[7] is the area of the South Atlantic (north of ca. 30°S) limited by the Equator. It usually has the opposite sign of the Southwestern Pole[7] (south of ca. 30° S) with southern limit at 50°S. This SST dipole-like pattern is positive when its phase consists of negative anomalies in the Northeastern Pole and positive anomalies in the Southwestern Pole and vice-versa for the negative phase[7]. It is possible to formulate an index for the SASD by subtracting the area-average SST of the Northeastern Pole from the Southwest Pole. This index can then be associated to precipitation variability over the continent.

In the Southern Hemisphere (SH), and particularly for the South Atlantic region, there is little evidence of Holocene millennial-scale events associated with cooler climate in the Northern Hemisphere (NH)[9]. Analysis of available proxy records for South America reveal, at the timing of these NH cold events, drier conditions in the equatorial region[10] and wetter conditions in the Andes[11] and central-eastern and southeastern Brazil[12]. In the South Atlantic Ocean, Mg/Ca SST records from the southwestern coast of Africa (25.3°S; 13.1°W)[13] are consistent with the variability of the $\delta^{18}O$ GISP2 record[14], while the foraminifera-derived SST from the western South Atlantic (25.5°S; 45.12°W)[15] follows the Antarctic Dome C variability[16]. Both have equivalent linear age-models

and confirm the presence of the Younger Dryas and a cooling event lasting from 8600−8000 years Before Present (yr BP) at both zonal boundaries of the subtropical South Atlantic. In the central South Atlantic (37.24°S; 12.28°W)[17], enhanced precipitation is linked with increased SST during the NH cold events.

The mechanisms of this relationship between Holocene abrupt climatic events in the South Atlantic SST and precipitation in South America are still unknown. Therefore, considering the strong relationship between the SASD and changes in the South Atlantic SST patterns, we reconstruct a SASD-like index for the Holocene using both proxy- and model-based approaches. We present for the first time a SASD-like index that is able to capture in the South Atlantic Basin the significant Holocene cold events observed in the NH and relate it with precipitation in South America for the last 12 kyr. It should be noted that the SASD is an inter-annual climate mode that starts to develop in austral spring, peaks in the summer, and decays in fall. Therefore, the variability associated with the SASD discussed in this paper is regarded as SASD-like variability.

## Results

The location of the proxy records used here is shown in Fig. 1a. From the proxy reconstruction of the SASD-like index ($SASD_{PROXY}$, Fig. 2) we can see that the $SASD_{PROXY}$ variability changes along the Holocene (for details of SASD-like index computation, see Methods Section) with higher-frequency behavior in the very early-Holocene (12−10 kyr BP) and very late Holocene (last 1 kyr). $SASD_{PROXY}$ also confirms the cold events observed in the NH with the same sign[9].

It should be noted that even though the location of the western Atlantic core is at the edge of the sign change in the spatial pattern of the SASD-like mode, when $SST_{WEST}$ obtained from the LaPAS-KF02[15] core is plotted against $SST_{EAST}$ from the Eastern Atlantic core ODP-1084B[13] the out-of-phase relationship of the SASD-mode is obtained. The time series were normalized by their standard deviation (Fig. 1b); the out-of-phase relationship that emerges suggests the influence of a SASD-like mode.

$SASD_{PROXY}$ and $SASD_{REC}$ (SASD-like index model-based reconstruction, see Methods Section) are shown in Fig. 3 together with the net solar flux and December insolation at 30°S. We see that $SASD_{PROXY}$ is in excellent agreement with $SASD_{REC}$. Both confirm for the South Atlantic the periods of rapid cooling associated with melt water pulses in the early Holocene, which include significant NH cold events (e.g. Younger Dryas and the response to the melt water pulse in 9−8 kyr). Both indices show a stable mid-Holocene period and a late Holocene peak. While the variability of the early Holocene is primarily driven by melt water discharge and changes in the ocean circulation, the late Holocene is thought to be driven predominantly by the solar forcing[9,18].

The time series for the three different formulations of the model-obtained SASD index are shown in Fig. 4. $SASD_{AVG}$ was calculated from area-averaged SST and $SASD_{EOF}$ was derived from the Principal Component of the 2nd EOF mode (see Methods Section).

The correlation coefficient (significant at 95% confidence level) between $SASD_{REC}$ and $SASD_{AVG}$ is 0.79 while that between $SASD_{EOF}$ and $SASD_{AVG}$ is 0.67. Therefore, for the last 12 kyr our $SASD_{REC}$ index can be related to the EOF mode of SST in the South Atlantic, which is equivalent to the $SASD_{AVG}$ approach[7].
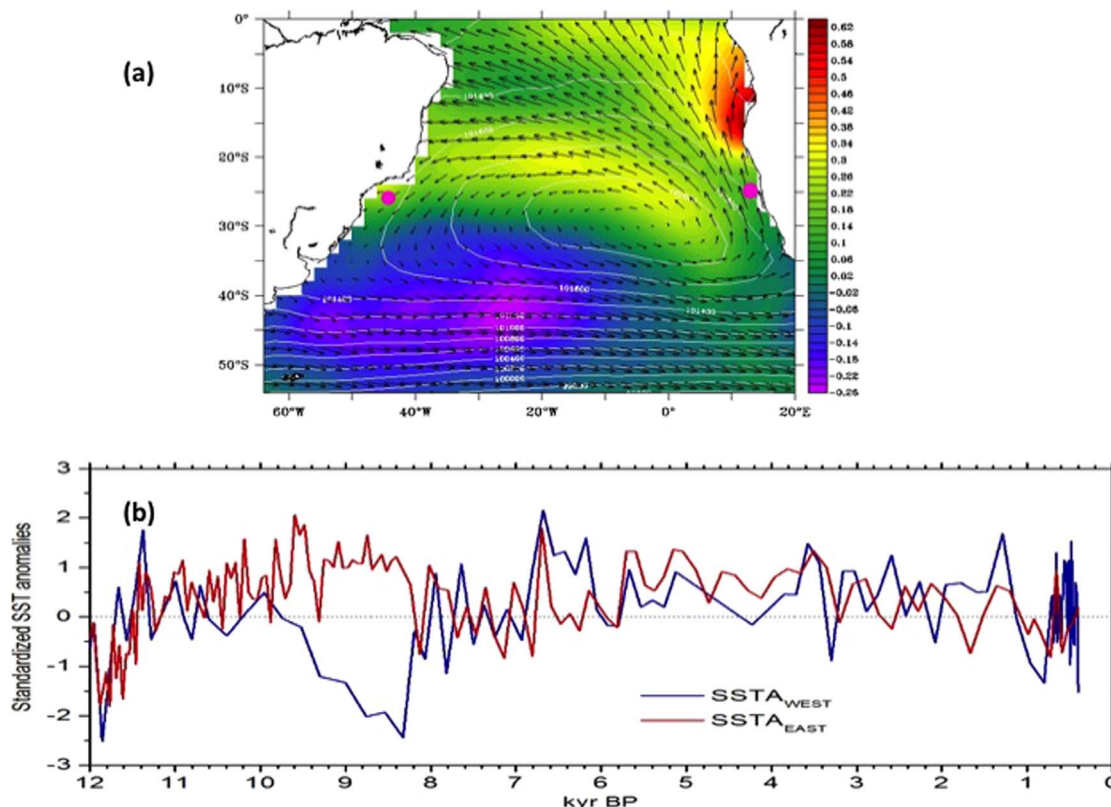


Figure 1 | (a) Core locations (pink circles, see Table 1 for core details) in the South Atlantic together with the spatial distribution of climatological mean sea level pressure and winds over the spatial representation of the spatial variability for Present Day through Empirical Orthogonal Function analysis (EOF). Shading colors refer to modern SST dominant (1st) EOF spatial mode from National Oceanic and Atmospheric Administration National Climatic Data Center Extended Reconstruction Sea Surface Temperatures, NOAA NCDC ERSST[34]. Contours are sea level pressure (Pa) 30 years climatology (1961–1990) with associated climatological wind (m/s) vectors superimposed. Both data locations are affected by changes in the Subtropical High system. (b) Annual mean SST time-series normalized by the standard deviation obtained from core LaPAS-KF02[15] in the western Atlantic (blue, $SSTA_{WEST}$) and from core ODP-1084B[13] in the eastern Atlantic (red, $SSTA_{EAST}$). Figure created with Ferret software.
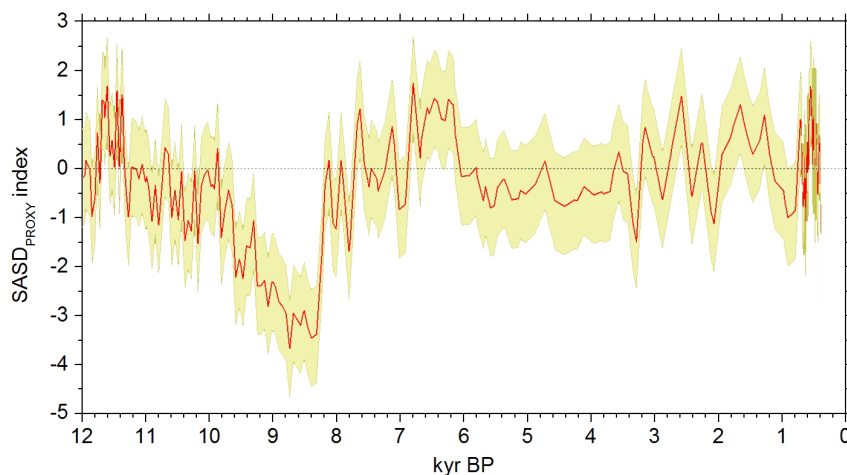
**Figure 2 | South Atlantic Subtropical Dipole proxy-reconstructed index (SASD$_{PROXY}$) for the last 12 kyr (red line).** The index was obtained by subtracting the standardized SST anomalies obtained from the Mg/Ca-derived SST record of the Northern Cape Basin[13] from foraminifera-based SST record at the southeastern Brazilian Continental upper slope[15] (Fig. 1b). See Table 1 for more details on the proxy records. Yellow shaded area corresponds to one standard deviation. Figure created with Origin software.

## Discussion

Since SASD$_{REC}$ is able to confirm the variability and changes of SASD$_{PROXY}$, we can derive the relationship between South Atlantic SST and precipitation in South America during the Holocene. Speleothem records from central-eastern Brazil are able to associate wetter conditions to the NH cold event of 8.6−8.0 kyr BP and 4.8−4.5 kyr BP[12]. Data from a speleothem record in Northeastern (NE) Brazil[19] indicate wetter conditions at 2.8 kyr BP. On the other hand speleothem records at different latitudes in Southeastern (SE) and Southern Brazil[20] do not confirm the NH cold events. In fact, what we see are opposite conditions for the Younger Dryas (drier in SE and wetter in Southern Brazil) which agrees with SASD$_{PROXY}$.

Using the transient model results[21], we show in Fig. 5 the time series of the SASD$_{REC}$ superimposed on the time series of NE
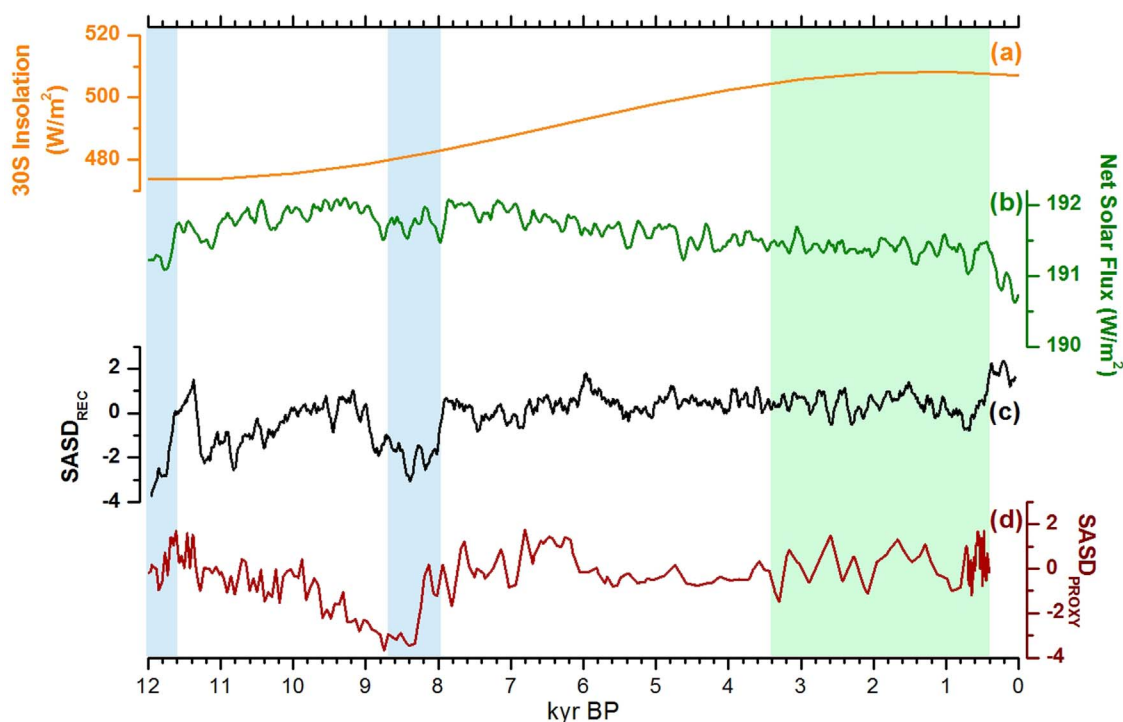


**Figure 3 | Variability of the reconstructed SASD index compared to the transient-model reconstructed SASD and the solar irradiance and solar insolation.** From the bottom to the top: (d) red curve is the standardized SST from proxy reconstructed SASD index (SASD$_{PROXY}$, i.e. Fig. 2) reproduced here for comparison with the (c) SASD index reconstructed from the transient model results[23], represented by black curve (SASD$_{REC}$). This index takes into account the exact location of the proxy-based SST data and follows its variability. The Younger Dryas and 8.6−8.0-kyr Northern Hemisphere cold events and the higher frequency variability in the late Holocene (marked by the blue and green vertical shading, respectively) are particularly noticeable. The green curve (b) shows the reconstructed solar irradiance from the model (W/m²); and (a), on the top in orange is the insolation for the month of December at 30°S[37] (W/M²). We can see that the solar irradiance accounts for the higher frequency variability of the SASD$_{PROXY}$ from 4 kyr to 0 kyr which is confirmed by the SASD$_{REC}$. The early Holocene is dominated by the fresh-water discharge, which coincided with a weaker solar insolation[9]. Figure created with Origin software.
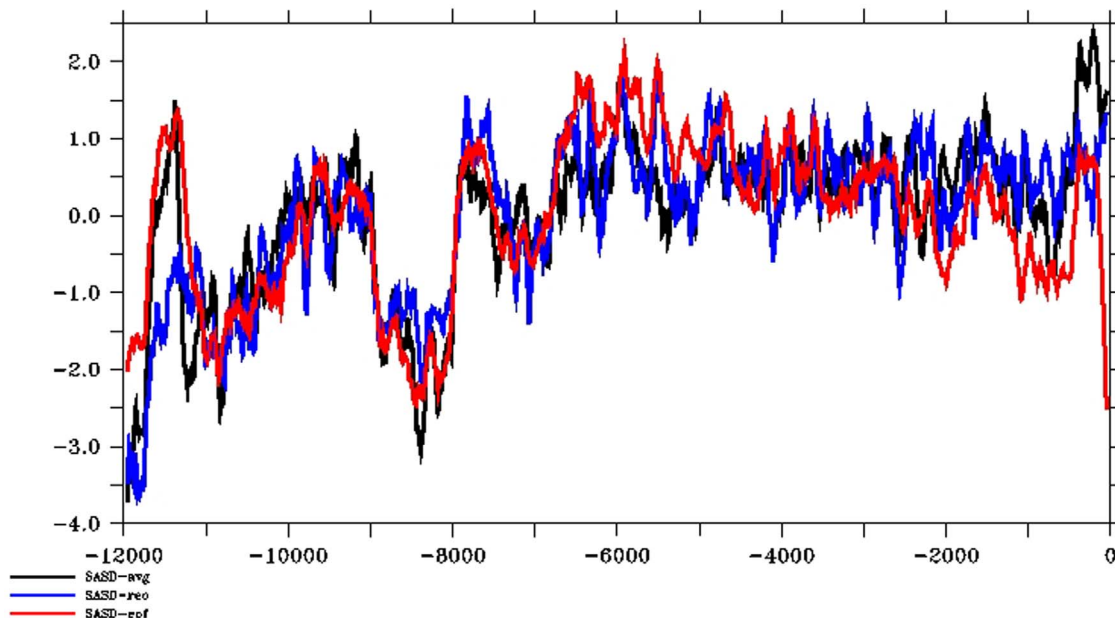
**Figure 4 | Time series for the different formulations of the SASD index based on the transient model for the past 12 kyr – see Methods Section.** Black line corresponds to the SASD$_{AVG}$, blue line corresponds to the SASD$_{REC}$, and red line corresponds to the time series of the SASD$_{EOF}$, which is the associated time series of the 2nd principal component (EOF). Figure created with Ferret software.
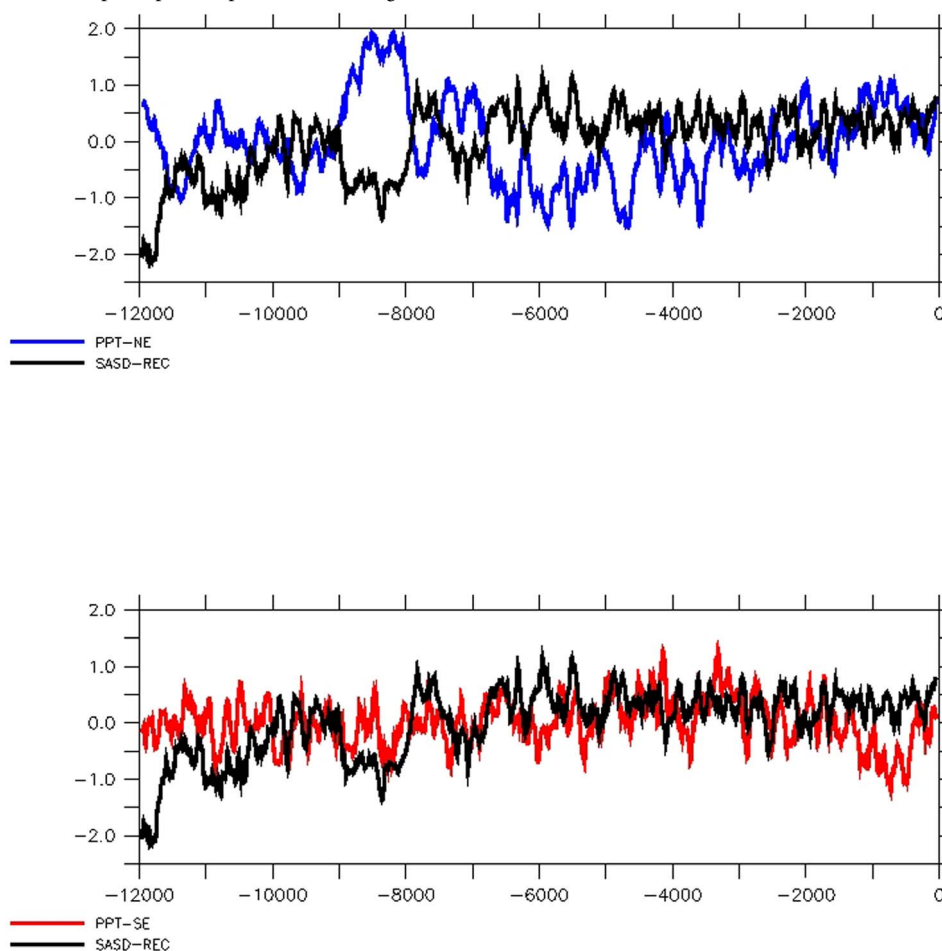




**Figure 5 | Relationship between precipitation in Northeastern and Southeastern Brazil with the South Atlantic Subtropical Dipole index.** SASD$_{REC}$ (blue solid line) and standardized precipitation-model anomalies in the last 12 kyr for (a) Northeastern Brazil (PPT-NE: 8°S-50°W, black solid line), and (b) Southeastern Brazil (PPT-SE: 30°S-55°W, red solid line). The regions were chosen according to the spatial variability pattern of modern day observed precipitation over South America. We see that the relationship between the South Atlantic Subtropical Dipole and the precipitation series from the two regions in Brazil have different behavior: PPT-NE shows a consistent out-of phase relationship which is not observed with PPT-SE indicating that there are other possible large-scale influences on the regional precipitation such as the ENSO signal. Figure created with Ferret software.
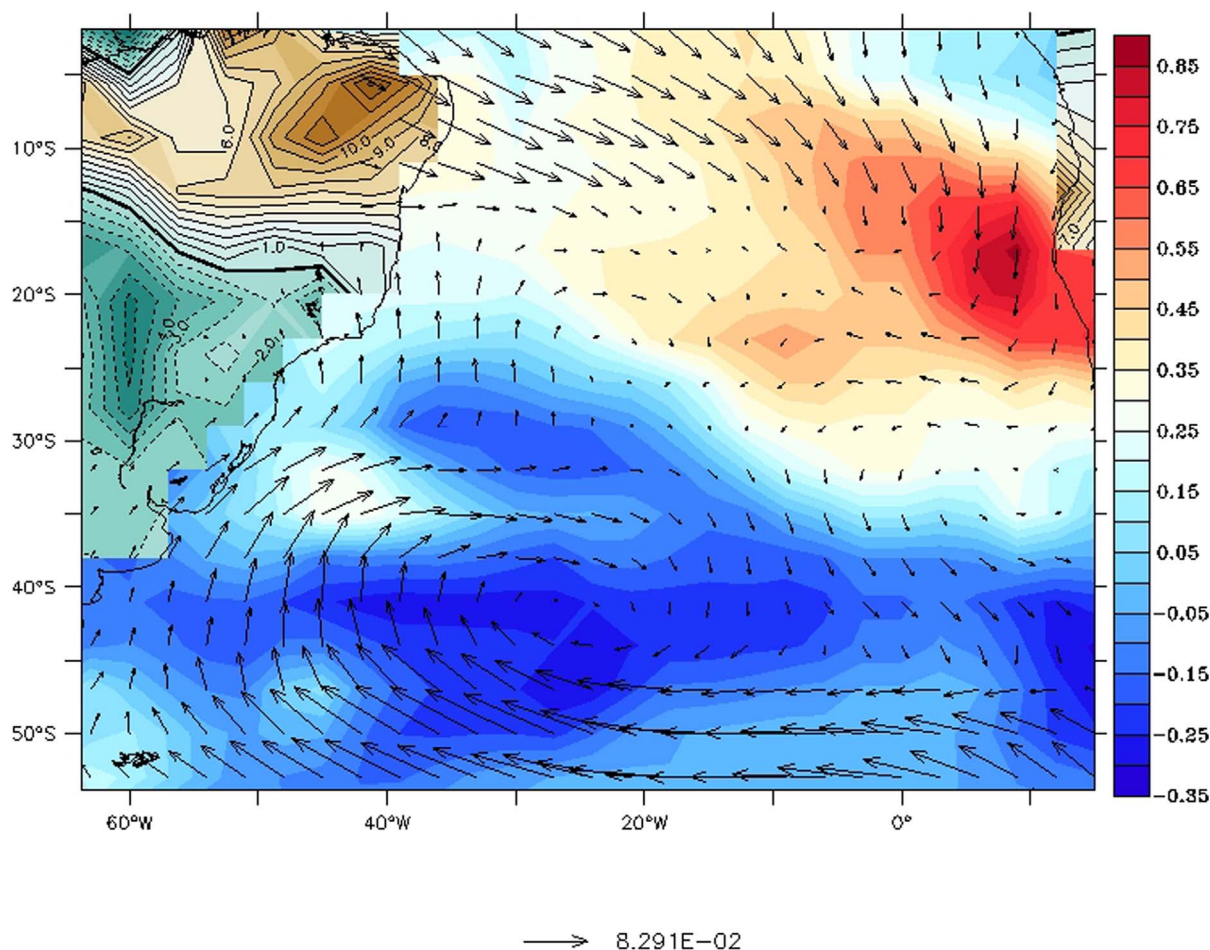
→ 8.291E-02

**Figure 6 | Composite differences between SASD$_{AVG}$ negative and positive years for SASD$_{AVG}$ below 2.0 and above 1.5 standard deviations.** SST (°C, color shading over the ocean), wind-stress (dyne/cm$^2$, vectors) and continental precipitation (brown and green shading with positive and negative black contours overlaid, mm/day). The SASD dipole, which is the dominant pattern of SST for the South Atlantic, emerges from the composite differences (in its negative phase) with negative differences in the Southwestern Pole and positive ones in the Northeastern Pole. The precipitation composite difference also shows a dipole pattern over South America. It displays wetter conditions (positive contours) for northern South America and drier conditions (negative contours) to the south. The composite differences in the wind-stress circulation strongly point the role of the South Atlantic in providing moisture for the wet Northeastern Brazil. Figure created with Ferret software.

precipitation (PPT-NE, 8°S-50°W, Fig. 5a) and SE precipitation (PPT-SE, 30°S-55°W, Fig. 5b). These two points were chosen based on the spatial pattern of the two first modes of Present Day (PD) variability of South American precipitation from Global Precipitation Climatology Centre (GPCC)[22], and are consistent with the seesaw pattern of South American precipitation[23,24]. From Fig. 5a a clear out-of-phase relationship between precipitation in NE Brazil and the SASD$_{REC}$ index is observed. This out-of-phase relationship shows that for the last 12 kyr, wetter (drier) conditions in NE were related to negative (positive) phases of the SASD$_{REC}$. In SE, PPT-SE and the SASD$_{REC}$ are mostly in phase. However, there are some periods when they are neither in nor out of phase, which could point to the role of ENSO on the precipitation regime over SE and Southern Brazil.

The proposed mechanism is that the negative (positive) SASD-like is associated with colder (warmer) waters in the Southwestern Pole

and warmer (colder) waters in the Northeastern Pole. This pattern corresponds to diminished (enhanced) evaporation in the Southwestern Pole and, consequently, decreased (increased) moisture advection to SE and Southern Brazil by the South Atlantic Subtropical High, resulting in drier (wetter) conditions in this region. Conversely, warmer (colder) waters in the SASD-like Northeastern Pole result in enhanced (diminished) evaporation in the tropical Atlantic, and wetter (drier) conditions in NE.

This is summarized in Fig. 6, which displays the composite difference of SST, surface wind stress over the ocean and continental precipitation averaged for the years when the SASD$_{AVG}$ is above 1.5 standard deviations and below 2.0 standard deviations. The SST spatial pattern that emerges is the SASD dipole in its negative phase, accompanied by a dipole pattern in the South American precipitation. The precipitation dipole displays wetter conditions (positive values) for northern South America and drier conditions

**Table 1 | Details of the paleo-records used in this study**

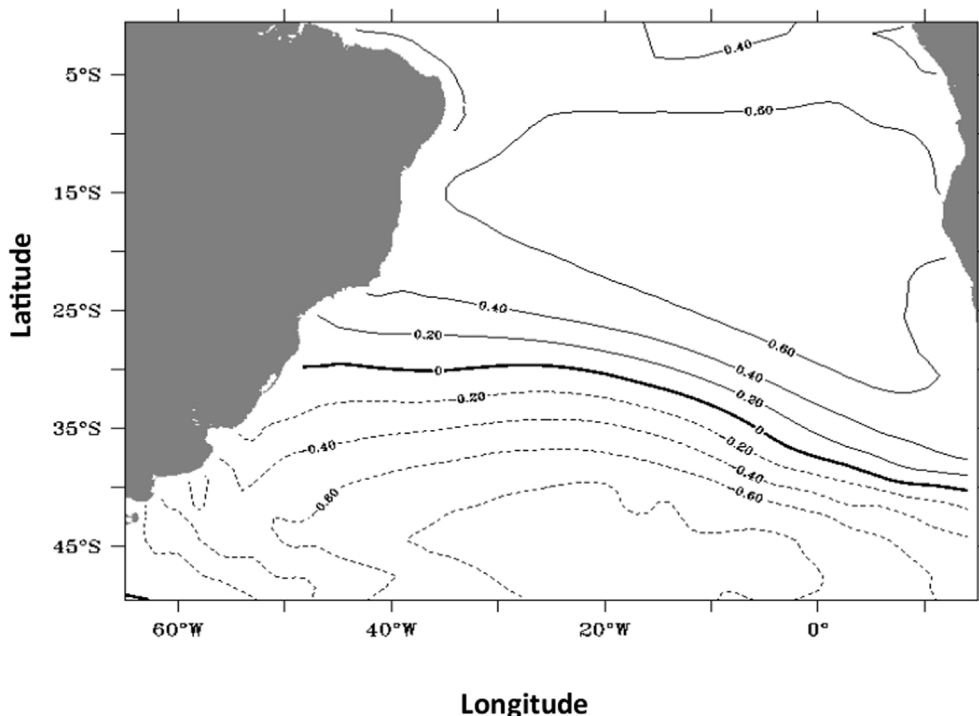| Core | Name | Latitude | Longitude | Depth (m) | Time (kyr) | Proxy |
|------|------|----------|-----------|-----------|------------|-------|
| LaPAS-KF02[15] | SSTA$_{WEST}$ | 25°50′S | 45°12′W | 827 | 0.402–12.958 | Planktonic foraminifera census counts |
| ODP-1084B[13] | SSTA$_{EAST}$ | 25°30′S | 13°1.67′E | 1992 | 0–21.262 | Mg/Ca ratio |

5

**Figure 7 | Correlation between the time coefficient of EOF1 (first) mode of SST and the SST spatial distribution over the South Atlantic Ocean for the 1850 Control Simulation with the NCAR-CCSM.** The skill of the NCAR-CCSM in reproducing the SASD was assessed as in[30]. Figure created with Ferret software.

(negative values) in the south. The composite difference in the wind stress circulation (overlain vectors in Fig. 6) strongly points to the role of the South Atlantic in providing moisture for the NE region. This leads to the conclusion that for the centennial-to-millennial time scale, the Younger Dryas and the 8.6−8.0 kyr NH cold event were characterized by wetter (drier) conditions in the Northeastern (Southern) Brazil relative to negative phase of the SASD index (colder Southwestern Pole and warmer Northeastern Pole), pointing to the key role played by the South Atlantic in driving South America precipitation variability.

## Methods

**Proxy-based data.** Two marine sediment cores in opposite sides of the South Atlantic were chosen to investigate the Northeast-Southwest dipole pattern in South Atlantic SST during the Holocene. Although the paleo-records were sampled around the same latitude their longitudes correspond to the east-west limit of the South Atlantic Basin (Fig. 1). The westernmost record was retrieved over the southeastern Brazilian Continental upper slope[15] and the easternmost was drilled over the continental slope in the Northern Cape Basin[13]. Both records consists of SST reconstructions and are located in regions largely impacted by changes in the Subtropical High regime, which is evident from the climatological representation of the winds and sea-level pressure shown in Fig. 1. These overlay the spatial structure for the modern South Atlantic SST dominant mode of
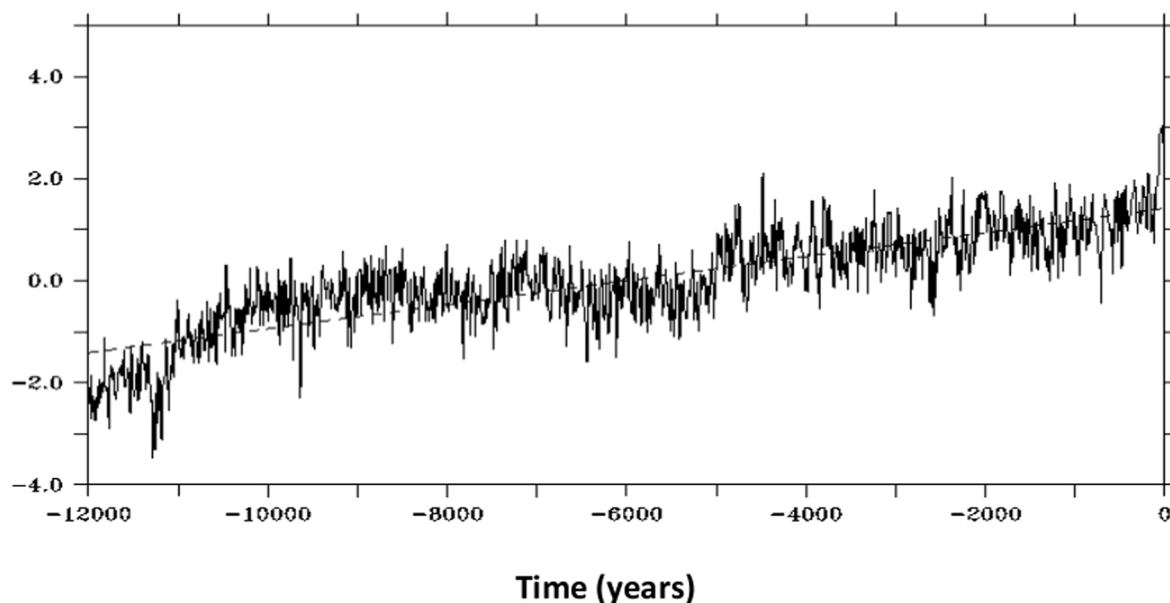


**Figure 8 | Time series associated with the first EOF mode of SST from the paleoclimate simulation with the global coupled model NCAR-CCSM considering the past 12,000 years, after the Younger Dryas cooling.** The linear trend line (dashed) is superimposed. Figure created with Ferret software.

variability (1st EOF) in rainbow-colored shading. Details of each record are shown in Table 1.

The analyzed core off the coast of Brazil was retrieved at the southeastern Brazilian Continental upper slope a depth of 827 m. The Brazil Current (BC) main flow is centered on the 1000 m isobath[25]. Although the region has some influence of the BC it should be noted that the record location lies within the upper slope of the middle/outer continental shelf, which puts the current's strongest flow away from the core location.

The core off the coast of Africa in eastern Atlantic[13] was retrieved at 1992 m water depth, about 300 km off the coast of Namibia over the continental shelf. The authors discuss the impact of the Benguela Current on the SST proxy data as one of many factors influencing its changes. They discuss that all of the factors controlling SST at the core location (e.g. changes in tropical winds impacting upwelling intensity and frequency, Benguela Current, Agulhas Current, etc.) have common roots in climate-mediated atmospheric and oceanic processes. It is pointed out that consistent climate patterns do emerge when comparing these temperature with other high-resolution tropical Atlantic paleoclimate records in the eastern Atlantic.

We reconstructed the SASD proxy index ($SASD_{PROXY}$) for the Holocene period by subtracting the proxy-based SST standardized time series of [13] from[15]. The $SASD_{PROXY}$ is shown in Fig. 2.

**Model-based index.** Results from a transient paleoclimate simulation with the global coupled model, the Community Climate System Model version 3 (CCSM3), maintained at the National Center for Atmospheric Research (NCAR) were also used in this study, aiming to physically interpret the analysis of the paleo-records. The simulation started at the Last Glacial Maximum (LGM, 21 kyr BP) and was run to pre-industrial times. The model used is the same as in the DGL-A experiment[24] but extended to pre-industrial times[26]. LGM reconstructions[27] are used as initial conditions as well as the varying concentrations of greenhouse gases ($CO_2$, $CH_4$ and $N_2O$)[28]. The coastlines and ice sheets volume variability are from ICE-5G database[29]. This numerical simulation includes melt water from NH and SH sources[30].

Three other formulations for the SASD index are calculated for the past 12 kyr based on the transient model results. First, we calculated the SASD index by subtracting the area-averaged SST at $30°$–$10°W$; $30°$–$40°S$ from the area-averaged SST at $20°W$–$0°$; $15°$–$25°S$[7] ($SASD_{AVG}$). Secondly, we calculated the Empirical Orthogonal Function Analysis (EOF)[31] of the South Atlantic SST.

In order to evaluate how well the NCAR-CCSM can capture the SASD mode we use the same method described in[32]. The authors evaluate the skill of several climate (CMIP3) models in reproducing SASD by performing EOF analysis of SST and correlating the associated time-series of the SASD mode with the South Atlantic Ocean SST monthly anomalies (their Fig. 1). Fig. 7 shows the correlation between the time coefficient of the first EOF mode SST and SST over the South Atlantic Ocean for an 1850 (pre-industrial) Control Simulation. The documentation of the 1850 control simulation can be found in[33]. The extension of the 1850 long (1300-years) CCSM control simulation[34] allows us to evaluate how the statistics of the climate mode has responded to the combined external forcings of the transient Holocene run. EOF1 for the past 12 kyr of the 21 kyr transient simulation represents the known warming trend since the Younger Dryas cooling[35] (The associated time-series and linear trend are shown in Fig. 8).

The second mode (EOF2) of the transient simulation results for the past 12 kyr reproduces the SASD pattern[6,7], and represents 24.9% of the explained variance. It reproduces the spatial structure of the modern day South Atlantic mode of variability shown in Fig. 1 from the NOAA-ERSST SST product[36]. The associated time series is used as a representation of the SASD index ($SASD_{EOF}$). Lastly, we calculated the SASD index from the model results based on the proxy-data locations by extracting the model SST time series at the exact same locations of the proxy-based SST records ($SASD_{REC}$).

1. Vera, C. et al. Toward a unified view of the American monsoon systems. J. Climate **19**, 4977–5000 (2006).

2. Marengo, J. et al. Recent developments on the South American monsoon system. Int. J. Climatology **32**, 1–21 (2012).

3. Liebmann, B. & Mechoso, C. The South American monsoon system. Global Monsoon System: Research and Forecast. Edited by Chang, C.-P., Ding, Y., Lau, N.-C., Johnson, R. H., Wang, B. & Yasunari, T. World Scientific, **2nd ed.**, 137–157 (2011).

4. Kayano, M. T., Andreoli, R. V. & Ferreira de Souza, R. A. Relations between ENSO and the South Atlantic SST modes and their effects on the South American rainfall. Int. J. Climatology **33**, 2008–2023 (2013).

5. Taschetto, A. & Wainer, I. The impact of the subtropical South Atlantic SST on South American Precipitation. Ann. Geophys. **26**, 3457–3476 (2008).

6. Haarsma, R. J. et al. Dominant modes of variability in the South Atlantic: A study with a hierarchy of ocean-atmosphere models. J. Climate **18**, 1719–1735 (2005).

7. Morioka, Y., Tozuka, T. & Yamagata, T. On the growth and decay of the Subtropical Dipole mode in the South Atlantic. J. Climate **24**, 5538–5554 (2011).

8. Nnamchi, H. C., Li, J. & Anyadike, R. N. C. Does a dipole mode really exist in the South Atlantic Ocean? J. Geophys. Res. **116** (2011).

9. Wanner, H., Solomina, O., Grosjean, M., Ritz, S. P. & Jetel, M. Structure and origin of Holocene cold events. Quaternary Sci. Rev. **30**, 3109–3123 (2011).

10. Haug, G. H., Hughen, K. A., Sigman, D. M., Peterson, L. C. & Rohl, U. Southward migration of the Intertropical Convergence Zone through the Holocene. Science **293**, 1304–1308 (2001).

11. Baker, P. A., Fritz, S. C., Garland, J. & Ekdahl, E. Holocene hydrologic variation at Lake Titicaca, Bolivia/Peru, and its relationship to North Atlantic climate variation. J. Quaternary Sci. **20**, 655–662 (2005).

12. Stríkis, N. et al. Abrupt variations in South American monsoon rainfall during the Holocene based on a speleothem record from central-eastern Brazil. Geology **39**, 1075–1078 (2011).

13. Farmer, E. C., DeMenocal, P. B. & Marchitto, T. M. Holocene and deglacial ocean temperature variability in the Benguela upwelling region: Implications for low-latitude atmospheric circulation. Paleoceanography **20**, PA2018 (2005).

14. Stuiver, M. & Grootes, P. M. GISP2 oxygen isotope ratios. Quaternary Res. **53**, 277–284 (2000).

15. Pivel, M., Santarosa, A., Toledo, F. & Costa, K. The Holocene onset in the southwestern South Atlantic. Palaeogeogr. Palaeocl. **374**, 64–172 (2013).

16. Jouzel, J. et al. Orbital and millennial Antarctic climate variability over the past 800,000 years. Science **317**, 793–796 (2007).

17. Ljung, K., Bjorck, S., Renssen, H. & Hammarlund, D. South Atlantic island record reveals a South Atlantic response to the 8.2 kyr event. Clim. Past. **4**, 35–45 (2008).

18. Jomelli, V. et al. Continuous 10,000-year long record of tropical Holocene deglaciation. Nature **474** (2011).

19. Novello, V. et al. Multidecadal climate variability in Brazil's Nordeste during the last 3000 years based on speleothem isotope records. Geophys. Res. Lett. **39**, L23706 (2012).

20. Cruz, Jr, F. W., Burns, S. J., Karmann, I., Sharp, W. D. & Vuille, M. Reconstruction of regional atmospheric circulation features during the late Pleistocene in subtropical Brazil from oxygen isotope composition of speleothems. Earth Planet. Sci. Lett. **248**, 495–507 (2006).

21. Liu, Z. et al. Transient simulation of last deglaciation with a new mechanism for Bølling-Allerød warming. Science **325**, 310–314 (2009).

22. Schneider, U. et al. GPCC's new land surface precipitation climatology based on quality-controlled in situ data and its role in quantifying the global water cycle. Theor. Appl. Climatol. **115**, 15–40 (2014).

23. Nogues-Paegle, J. & Mo, K. C. Alternating wet and dry conditions over South America during summer. Mon. Wea. Rev. **125**, 279–291 (1997).

24. Cavalcanti, I. F. A. Large scale and synoptic features associated with extreme precipitation over South America: A review and case studies for the first decade of the 21st century. Atmos. Res. **118**, 27–40 (2012).

25. Mahiques, Michel, M. et al. Sedimentary changes on the Southeastern Brazilian upper slope during the last 35,000 years. Anais Acad. Bras. de Ciências **79**, 171–181 (2007).

26. He, F. Simulating transient climate evolution of the last deglaciation with CCSM3. Ph.D. thesis, University of Wisconsin (2010).

27. Otto-Bliesner, B. L., Brady, E. C., Clauzet, G., Tomas, R., Levis, S. & Kothavala, Z. Last glacial maximum and Holocene climate in CCSM3. J. Climate **19**, 2526–2544 (2006).

28. Joos, F. & Spahni, R. Rates of change in natural and anthropogenic radiative forcing over the past 20,000 years. Proc. Natl. Acad. Sci. USA **105**, 1425–1430 (2008).

29. Peltier, W. Global glacial isostasy and the surface of the ice-age earth: The ICE-5G (vm2) model and GRACE. Ann. Rev. Earth Planet. Sci. **32**, 111–149 (2004).

30. Marson, J., Wainer, I., Liu, Z. & Mata, M. The impacts of melt water pulse-1a in the South Atlantic Ocean deep circulation since the last glacial maximum. Clim. Past Disc. **9**, DOI: 10.5194/cpd–9–6375–2013 (2013).

31. Lorenz, E. N. Empirical orthogonal functions and statistical weather prediction. Tech. Rep. 1, Statistical forecasting project, Dept. of Meteorology, MIT, Cambridge, USA. (1956).

32. Bombardi, R. J. & Carvalho, L. M. V. The South Atlantic dipole and variations in the characteristics of the South American Monsoon in the WCRP-CMIP3 multi-model simulations. Climate Dyn. **36**, 2091–2102 (2011).

33. Otto-Bliesner, B. L., Tomas, R., Brady, E. C., Ammann, C., Kothasvala, Z. & Clauzet, G. 2006: Climate sensitivity of moderate and low resolution versions of CCSM3 to preindustrial forcings. J. Climate **19**, 2567–2583.

34. Danabasoglu, G. & Gent, P. R. Equilibrium climate sensitivity: Is it accurate to use a slab ocean model? J. Climate **22**, 2494–2499 (2009)

35. Alley, R. B. The Younger Dryas cold interval as viewed from central Greenland. Quaternary Sci. Rev. **19**, 213–226 (2000).

36. Smith, T. M., Reynolds, R. W., Peterson, T. C. & Lawrimore, J. Improvements to NOAA's historical merged land-ocean surface temperature analysis (1880–2006). J. Climate **21**, 2283–2296 (2008).

37. Berger, A. & Loutre, M.-F. Insolation values for the climate of the last 10 million years. Quaternary Sci. Rev. **10**, 297–317 (1991).

## Acknowledgments

## Author contributions

I.W. and L.F.P. designed the study and undertook main analysis. I.W., L.F.P., M.K. and B.O.-B. discussed the results and contributed to the writing of the Manuscript.

## Additional information